Contents lists available at ScienceDirect

International Journal of Heat and Mass Transfer

journal homepage: www.elsevier.com/locate/hmt

Programmable all-thermal encoding with metamaterials

Min Lei [a], Chaoran Jiang [b,c], Fubao Yang [a], Jun Wang [d,e,f,*], Jiping Huang [a,*]

[a] *Department of Physics, State Key Laboratory of Surface Physics, and Key Laboratory of Micro and Nano Photonic Structures (MOE), Fudan University, Shanghai 200438, China*
[b] *Department of Physics, Chinese University of Hong Kong, Hong Kong 999077, China*
[c] *The Beijing Computational Science Research Center, Beijing 100193, China*
[d] *School of Physics, East China University of Science and Technology, Shanghai 200237, China*
[e] *School of Mathematics, East China University of Science and Technology, Shanghai 200237, China*
[f] *Wenzhou Institute, University of Chinese Academy of Sciences, Wenzhou 325001, China*

ABSTRACT

Advanced encoding technologies are crucial for information processing and storage, and have been widely studied and implemented in various wave fields such as electromagnetics and acoustics. However, heat has not been commonly utilized as a significant carrier of information due to the lack of programmability with flexible unit structures, which severely limits its practical applications. In this context, we first propose a novel programmable all-thermal encoding strategy that utilizes macroscopic conductive heat for digital encoding under purely thermal fields. Our approach leverages switchable cloak-concentrator metadevices to distinguish and modulate binary signals based on the divergent features of heat flows on each unit. The encoding operation is made programmable with the use of temperature-responsive phase change materials, which benefit from the self-adaptive external-stimulus and internal-response mechanism. To demonstrate the feasibility of our approach, we fabricate a proof-of-concept prototype using shape memory alloys that exhibit phase-change behavior under specific temperatures, resulting in a robust thermal encoding platform. This proposed scheme presents a practical paradigm for all-thermal logical metadevices and opens up new avenues for implementing modern information technologies in ubiquitous diffusion systems.

© 2023 Elsevier Ltd. All rights reserved.

1. Introduction

The development of modern encoding technology has made processing, encryption, and transmission of information possible [1]. The concept of encoding was first observed in nature, such as the encoding of sunlight by drops in the atmosphere to produce rainbows. With the growing demand for information transfer, encoding was introduced into human society [2,3]. In the past century, there have been groundbreaking advances in information science, mainly in the physical fields of light, sound, and electromagnetic waves [4,5]. Heat, as another carrier of information, is the main form of energy transport in the diffusion process that is ubiquitous in industrial production and daily life [6]. If heat can be utilized as another medium for information transmission and processing, it is promising to simultaneously address two long-standing issues in the electronic industry: heat dissipation and recycling.

The use of heat for encoding and logical calculation began with the manipulation of microscopic phonon motion [7,8]. By tailoring the nonlinear interaction between phonons, various counterparts of electronic devices were first proposed and then experimentally realized, such as thermal diodes, transistors, and memories [9–12]. However, analogs in macroscopic systems are still rare and incomplete, which limits the generalization of phononic regulation in macroscopic conduction processes. There mainly exist two obstacles to overcome. On the one hand, the physical mechanism of macroscopic heat diffusion is significantly different from the waves that govern electron or photon motion in classical encoding [13,14], making direct theoretical imitation challenging. On the other hand, a fundamental programmable prototype is lacking to provide a proof-of-concept platform. Fortunately, the recent rapid development of thermal metamaterials provides an opportunity to realize the encoding operation of macroscopic thermal signals through artificial structure design [15–30]. Heat can be localized and manipulated freely, regardless of its intrinsic diffusion
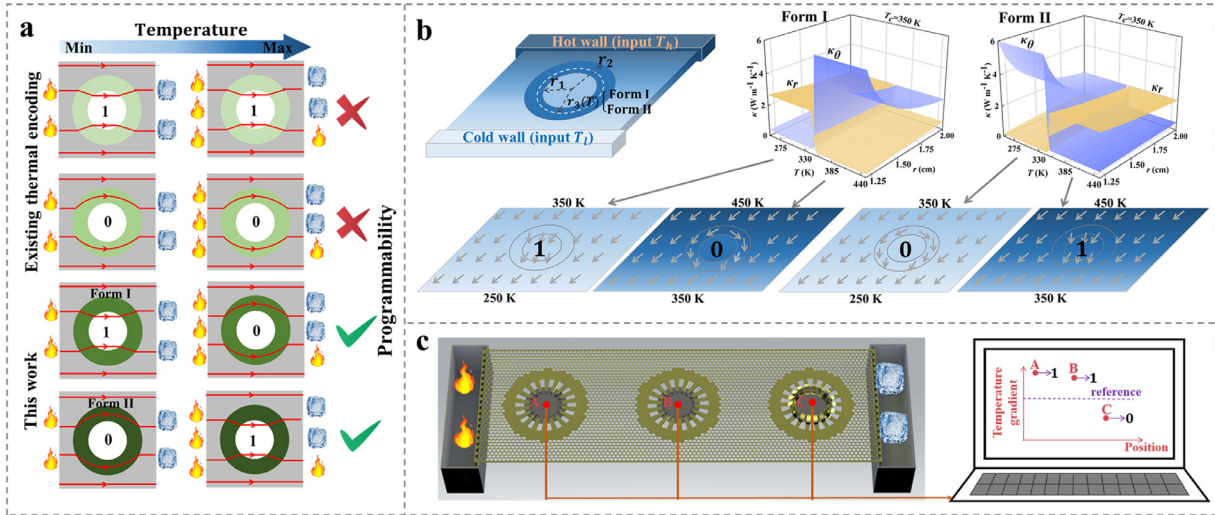

Fig. 1. Principle of programmable all-thermal encoding. (a) The existing thermal encoding equipment in the literature has a fixed output once the structure is given, and thus such equipment does not have programmability. In contrast, the encoding equipment reported in this work has programmability, namely, it can automatically adjust the output encoding value at different ambient temperatures. (b) The structure of a programmable all-thermal encoding unit. We use elements of two forms, Form I and Form II, with the same phase transition temperature and opposite phase transition directions. At low temperatures, the radial thermal conductivity of the Form I (Form II) unit is greater than (lower than) the tangential thermal conductivity, resulting in the concentrator (cloak) function and outputting a 1 state (0 state). At high temperatures, the function is reversed, with the Form I (Form II) unit functioning as a cloak (concentrator), and outputting a 0 state (1 state). (c) Two forms of units are arranged to form an encoding array. The encoded output is achieved by reading the temperature gradient value in the unit's center. If the temperature gradient value is higher (lower) than the reference value, the output is 1 (0).

nature. Nevertheless, programmability remains a challenging issue for further practical applications.

In this work, we present a universal all-thermal encoding scheme (corresponding to the concept of all-optical signal processing in optics) using temperature-responsive thermal metadevices [31–35]. We propose a basic theoretical framework with a temperature-controlled strategy. The state of the unit cell is programmed by adjusting its local temperatures, and the input/output of the signal is achieved by reading in/out local temperature gradients. Based on this mechanism, we design a series of thermal encoding metamaterials that work in both steady and transient environments. Using shape memory alloys with phase-change characteristics, we experimentally fabricate a temperature-controlled encoding platform and demonstrate its encoding process. Hu et al. [36] first proposed the thermal encoding functionality by manipulating the thermal cloaking and thermal concentrating units. Since then, the functional design of thermal encoding has become more diverse and intelligent [37,38]. Our work introduces switchable cloak-concentrator metadevices, which enable programmable encoding (as shown in Fig. 1(a)) and promote the practical application of existing encoding schemes. Additionally, our work overcomes the complexity of previous designs that required multi-field synergetic control [38] by providing a recipe for all-thermal modulation. This state-of-art platform verifies the feasibility of manipulating macroscopic heat flow for information encoding and opens a different door for logical computation with diffusion systems. Various functions of thermal metamaterials are also available in multi-field metamaterials, such as thermoelectric cloaks [39,40], thermoelectric concentration [41], and thermoelectric camouflage [42,43]. Hence, thermal encoding utilizing thermal metamaterials can present prospects for encoding design in multiphysical fields.

2. Theoretical design by transformation thermotics

Our aim is to achieve programmable all-thermal encoding, enabling an infinite number of encoded outputs for temperature control on a single device. To accomplish this, we use a nonlinear

metamaterial as the encoding unit, which can realize the function switch of the cloak and concentrator with temperature control. Under the premise of ensuring that the background heat flow is unchanged, the thermal cloak makes the heat flow bypass the middle area, and the thermal concentrator makes the heat flow gather through the middle area. We use the divergent values of heat flow between the central regions of cloak and concentrator to distinguish binary signals; bypassing corresponds to the 0 state, and concentrating corresponds to the 1 state. The encoding unit cells based on a switchable cloak-concentrator will produce different output digital states under varying ambient temperatures, as shown in Fig. 1(b).

Temperature-dependent transformation thermotics [31] can achieve switchable cloak-concentrator. According to Fourier's law, governing equation of heat conduction without a heat source can be described as

$$\rho C \frac{\partial T}{\partial t} = \nabla \cdot (\boldsymbol{\kappa} \cdot \nabla T), \tag{1}$$

where ρ and C are density and thermal capacity, $\boldsymbol{\kappa}$ is temperature-independent thermal conductivity tensor, and T is temperature. According to temperature-dependent transformation thermotics [31], form of heat conduction equation remains unchanged after temperature-dependent coordinate transformation (see Appendix A1 for proof). Thus transformed thermal conductivity, density, and thermal capacity can be expressed as

$$\boldsymbol{\kappa}'(T') = \frac{A(T)\kappa_0 A^{tr}(T)}{\det A(T)},$$
$$\rho'(T) = \frac{\rho}{\det A(T)},$$
$$C' = C, \tag{2}$$

where $\boldsymbol{\kappa}'(T)$ is temperature-dependent thermal conductivity of device, κ_0 is temperature-independent thermal conductivity of background, $A(T)$ is a temperature-dependent Jacobian matrix determined by a coordinate transformation, $A^{tr}(T)$ is transpose of $A(T)$, and $\det A(T)$ is determinant of $A(T)$. The transformed thermal capacity in Eq. (2) remains unchanged after a coordinate transfor-

mation, and the transformed density is only related to $\det A(T)$. In steady state, $\frac{\partial T}{\partial t} = 0$, regardless of density and thermal capacity.

Temperature-dependent coordinate transformations accomplish the functional switching characteristics of nonlinear metamaterials. At polar coordinates, the temperature-dependent coordinate transformations can be written as

$$r' = r_1 r / r_3(T) \quad (r' < r_1),$$
$$r' = r(r_2 - r_1)/(r_2 - r_3(T)) + r_2(r_1 - r_3(T))/(r_2 - r_3(T)) \quad (r_1 < r' < r_2),$$
$$\theta' = \theta, \tag{3}$$

where r_1 and r_2 are the inner radii and outer radius of the transformation region of the encoding unit, see Fig. 1(b). Eq. (3) corresponds to the coordinate transformation of the concentrator when $r_3(T) = r_3$ (where r_3 is between r_1 and r_2). If $r_3(T) = 0$, Eq. (3) corresponds to coordinate transformation of cloaks. Thus, $r_3(T)$ is necessary to implement a temperature-controlled phase transition between r_3 and 0, so that the encoding unit can switch functions between the cloak and the concentrator.

We consider two forms of the unit to provide more freedom for adjustment. The temperature-dependent radius $r_3(T)$ has two forms which can be written as

$$r_3(T) = \frac{r_3}{1 + \exp \eta (T - T_C)} \quad \text{(Form I)},$$

$$r_3(T) = \frac{r_3 \exp \eta (T - T_C)}{1 + \exp \eta (T - T_C)} \quad \text{(Form II)}, \tag{4}$$

Here, T_C is the critical temperature around which $r_3(T)$ can be distinguished by 0 or r_3. We can obtain two types of thermal encoding units corresponding to Form I and Form II, as depicted in Fig. 1(b). For Form I (Form II), the temperature-dependent radius $r_3(T)$ is 0 (r_3) when the ambient temperature is higher than T_C, and $r_3(T)$ is r_3 (0) when the ambient temperature is lower than T_C. By substituting Eq. (3) into Eq. (2), we obtain the transformed thermal conductivity and density of the entire unit structure (refer to Appendix A1 for details). The function of the unit is determined by the ratio of radial and tangential thermal conductivity. We illustrate the phase diagram of two types of phase-change materials in Fig. 1(b), where the critical temperature T_C is set to 350 K. The thermal conductivity of Form I (Form II) unit $\kappa_r < \kappa_\theta$ ($\kappa_r > \kappa_\theta$) corresponds to thermal cloak (concentrator) when the unit temperature is higher than the critical temperature. When the temperature is below the critical temperature, $\kappa_r > \kappa_\theta$ ($\kappa_r < \kappa_\theta$) corresponds to thermal concentrator (cloak). The two forms of units have the same phase transition temperature but opposite phase transition direction. The simulation results are presented in Fig. A1 (Appendix).

The encoding units of the switchable cloak-concentrator are arranged to form the encoding array. We read the temperature gradient values of the central and background regions of each cell to achieve the encoded output. The temperature gradient value of the background area serves as the reference value, and the temperature gradient value of the central region, which is higher (lower) than the reference value, corresponds to the function of the concentrator (cloak), and the output is 1 state (0 state). In this way, we can use the encoded array to achieve a sequence of encoded output values, as shown in Fig. 1(c). By adjusting the temperature of the encoding array, we can realize a new encoding output, allowing a single device to record many, or even unlimited, output values.

3. Numerical simulations under two cases

3.1. Steady case

We use finite-element simulation software COMSOL Multiphysics [44] to demonstrate programmable all-thermal encoding

under steady-state conditions, as shown in Fig. 2. The dimensions of the whole plane are 10×60 cm^2, with the background thermal conductivity of all units being 1 W m^{-1} K^{-1}. Each encoding unit in Fig. 2 has an inner radius of $r_1 = 1$ cm, an outer radius of $r_2 = 2$ cm, and a virtual radius of $r_3 = 1.5$ cm. The encoding array, consisting of these units, can be manipulated individually and in batches, as shown in Fig. 2(a) and (c), respectively. Individual manipulation refers to the manipulation of the temperature for each unit in the encoded array. The six units of Form I are arranged in a one-dimensional array along the horizontal direction, with a critical temperature of 350 K and a bottom boundary temperature of 300 K. The left and right boundaries of every unit are insulated, ensuring no heat exchange between units. The output state of each unit can be adjusted individually by assigning each unit a different upper boundary temperature, and the relationship between the input temperature and the output state is established. Figure 2(a) demonstrates all units becoming concentrators (cloaks), with outputs of 1 (0) when the upper boundaries are set to 340 K (450 K) lower (higher) than the critical temperature. The 0 and 1 states appear interleaved in the encoded array in Fig. 2(a) III. Each unit can achieve a 0 state and a 1 state in individual manipulation because the units do not affect each other. The six-unit encoded array can achieve a total of 2^6 output species. In separate manipulation, the encoding array can consist of units of Form II, or even a mixture of units of the two forms, to achieve different encoding outputs under the same conditions (see Appendix A2 for details). Figure 2(c) demonstrates a batch control strategy that fixes the low temperature at the right boundary and gradually increases the high temperature at the left boundary. Upper and lower boundaries are set to be insulated. Here we use six units to form the encoded array, including two corresponding to Form II and four corresponding to Form I. The encoded output value is (0,1,0,0,1,1) when the left boundary temperature is 400 K. As the temperature of the left boundary gradually increases, the output value changes from (0,1,0,1,1,1) to (0,1,0,1,0,1). Batch operations are simple; you only need to control two inputs to achieve multiple encodings. An encoding array consisting entirely of units of Form I or units of Form II can also change one input to achieve multiple encoding outputs in batch manipulation (see Appendix A3 for simulation results). The batch operation helps to perform large-scale operations on some codes requiring step changes in practical applications. In short, both controls allow the array to achieve multiple outputs, and the temperature can be adjusted to achieve reprogrammable encoding of a fixed structure.

Measuring the temperature gradient at the central site is a more precise and efficient way to obtain the signal output than directly observing the temperature profile. To do this, we extract the temperature gradient at the central site and background of each unit in Fig. 2(a) and (c) to create the temperature gradient-position curve, as shown in Fig. 2(b) and (d). The 0 and 1 states are highly distinguishable in the curves. We use the background temperature gradient as the reference value. The temperature gradient values at the central site of the cloak corresponding to the 0 states are almost zero and lower than the reference value, while the temperature gradient values of the concentrator corresponding to the 1 state are all higher than the reference value. The phase transition temperature T_C is used to distinguish the input temperature. Inputs below T_C produce only one output, while inputs above T_C produce another output. We have verified the robustness of this approach in simulations, and different input temperatures do not affect the final output results under conditions far from T_C.

3.2. Transient case

We perform a transient simulation on the encoded arrays operated in batches and individually. We select the simulation results
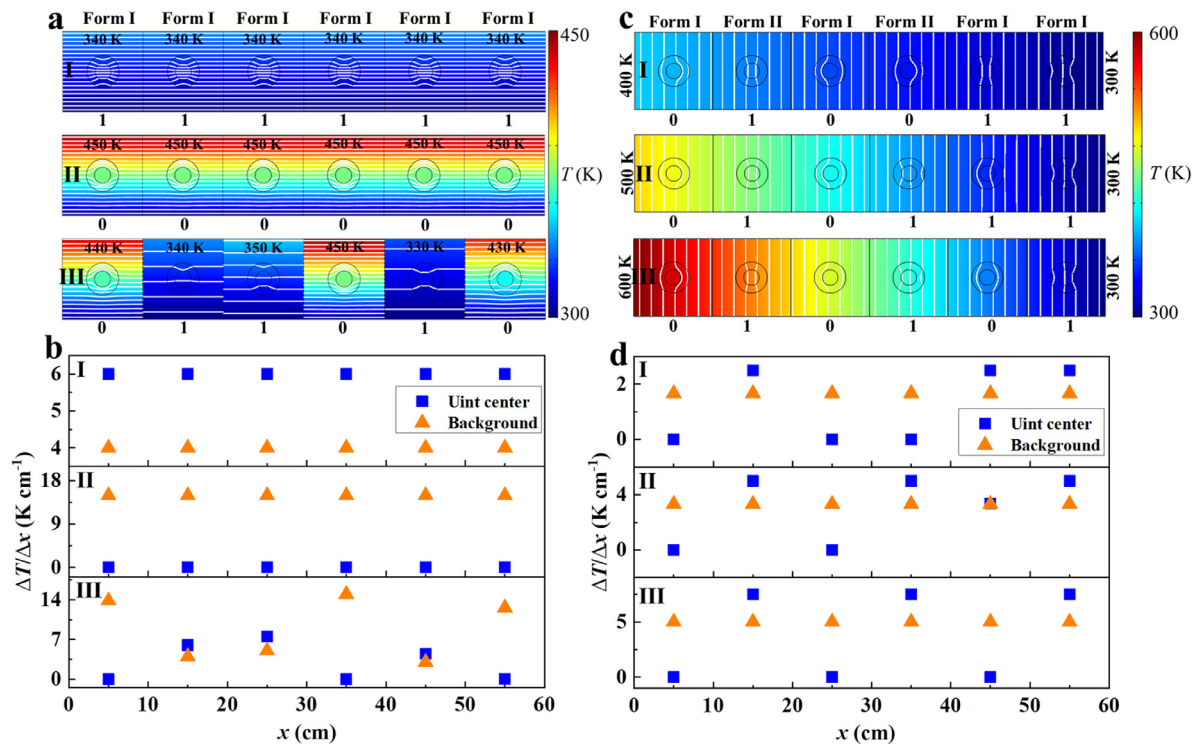
Fig. 2. Simulation results of individual and batch manipulations of encoded arrays in steady state. (a) The simulation result in which the encoded array is manipulated individually. The left and right boundaries of each unit are thermally insulated. The lower boundaries are set at 300 K thermally. (c) The simulation results of batch control of encoding array. The upper and lower of each unit are thermally insulated. (b) shows the temperature gradients of units' center and background in (a), and (d) corresponds to (c).

at four moments respectively for display, as shown in Fig. 3(a) and (c). The size parameters and background thermal conductivity of each encoding unit in Fig. 3 are the same as those in Fig. 2. We extract temperature gradient data of each unit's central site and background at four moments and plot the temperature gradient-position curve, as shown in Fig. 3(b) and (d). For individual manipulation, we set the bottom boundaries of the separately operated units to 300 K and the upper boundaries individually to 340 K lower than the critical temperature ($T_C = 350$ K) and 450 K higher than the critical temperature. We set the initial temperature of the initial state to a low temperature of 300 K, resulting in an output of 1 state for all units. Units 2, 4, and 6 with low-temperature boundary conditions always produce an output of 1, while units 1, 3, and 5 with high-temperature boundary conditions initially produce an output of 1 and then transition to 0. As shown in Fig. 3(b), the temperature gradient values of units with high-temperature boundaries (units 1, 3, and 5) undergo significant changes, showing the change process from concentrators to cloaks. However, the temperature gradient values of units with low-temperature boundaries (units 2, 4, and 6) change little during the evolution process. To determine the final output value of a unit, we repeatedly detect the temperature during the evolution from the initial state to the steady state after initializing the entire system. If we observe the output value of a unit change from 1 to 0 during detection, we can predict the final output value will be 0; otherwise, it will be 1. For batch control, the final output cannot be predicted in advance since each unit's output is not separate. As time increases, the high temperature is gradually transferred to the right, and the temperature perceived by the encoding unit increases. The encoding unit responds to local temperature variation, and the result of the encoding array changes with time, from (0,1,0,0,1,1) to (0,1,0,1,0,1). Without changing the input conditions, a batch-controlled device produces multiple output results, achieving repeatability encoding.

Thus, we demonstrate that transient encoding arrays can output multiple encoding results individually or in batches. As shown in Fig. 3(c), the thermal encoding array operated in batches can only produce stable encoding values after 800 s, which is a lengthy process. The speed of thermal encoding output can be increased by utilizing materials with high diffusivity or by applying real-time prediction methods for transient encoding.

4. Experimental realization by scattering cancellation technology

4.1. Experimental design

Achieving perfect cloaks and concentrators using temperature-dependent transformation thermotics requires material parameters with high requirements, such as anisotropy, inhomogeneity, and singularities in space. These factors greatly restrict the fabrication of actual devices. To overcome this limitation, we propose constructing nonlinear encoding units with a bilayer structure based on temperature-dependent scattering cancellation theory. Previous studies have reported linear bilayer cloaks and concentrators that use two layers of isotropic materials to achieve cloaking and concentrating functions [45–47], which anisotropic materials can achieve. To realize the switch between the cloak and the concentrator, we combine the thermal conductivity characteristics of the bilayer thermal cloak and the bilayer thermal concentrator and introduce nonlinear materials. A schematic diagram of the bilayer structure encoding units is shown in Fig. 4(a). The inner, middle, and outer radii of the bilayer ring structure are defined as R_0, R_1, and R_2, which are determined constants. The thermal conductivities of the materials from region 1 to region 4 are κ_0, $\kappa_1(T)$, κ_2, and κ_b. The thermal conductivity of region 2 must be able to switch between an on (high)/off (low) state in real-time
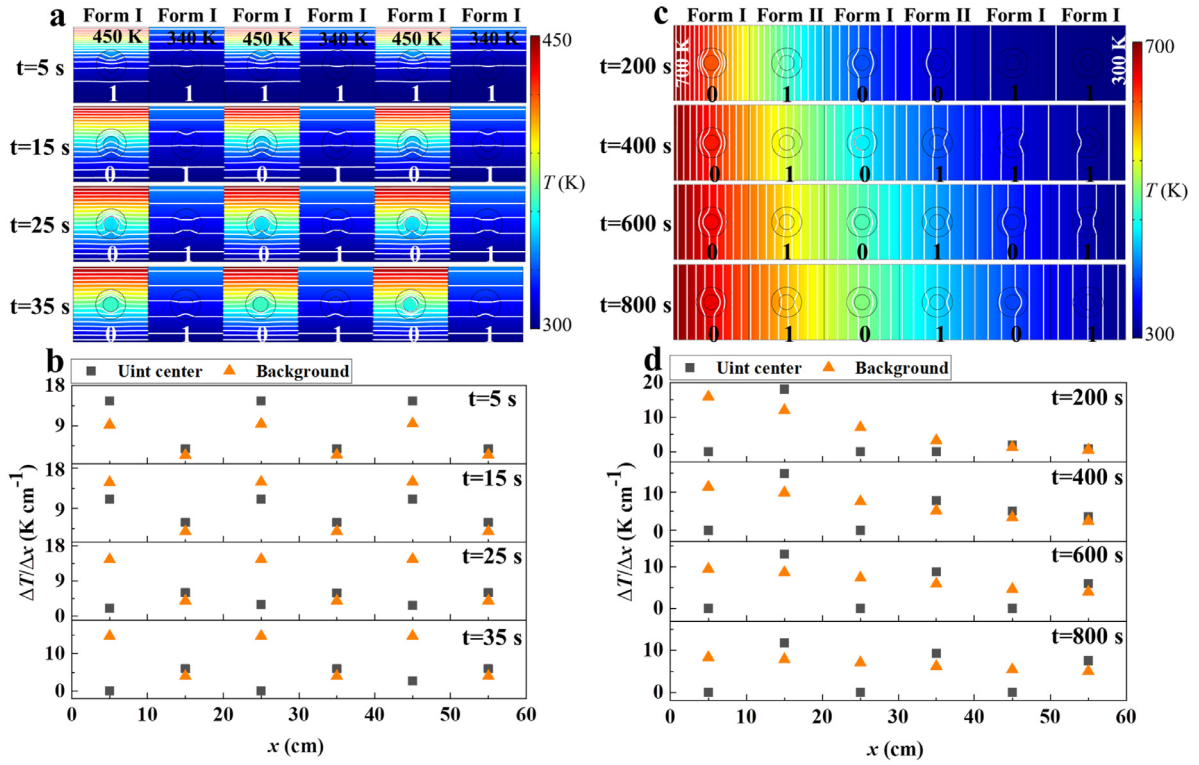
Fig. 3. Transient simulation results for individual and batch manipulation of encoded arrays. (a) The output results of the encoding array with each unit individually temperature-controlled at different times. Insulate the left and right boundaries of each unit. The lower boundaries are set at 300 K thermally. (c) The output results from batch manipulation encoding arrays at different times. The upper and lower boundaries of each unit are insulated. (b) and (d) denote the evolution of the temperature gradient values at the unit center and background over time, corresponding to (a) and (c).

in response to external stimuli, such as electric field [48], magnetic field [49–51], electrochemistry [52], light field [53], and pressure [54,55]. To achieve full thermal control of the encoding unit, we use a temperature phase change material that can switch the thermal conductivity without introducing additional fields. Here $\kappa_1(T)$ has two switching forms, corresponding to units of Form I and Form II, respectively, it can be set to

$$\kappa_1(T) = \frac{\kappa_1}{1 + e^{T-T_C}} \quad \text{(Form I)},$$

$$\kappa_1(T) = \frac{\kappa_1 e^{T-T_C}}{1 + e^{T-T_C}} \quad \text{(Form II)}, \tag{5}$$

where T_C is phase transition temperature, which can be given according to nature of materials. The thermal conductivity $\kappa_1(T)$ jumps between 0 and κ_1, where 0 corresponds to the parameter requirements of the cloak and κ_1 is a constant.

Given the background thermal conductivity κ_b, the thermal conductivity of region 3 satisfying the parameter requirements of the bilayer thermal cloak can be calculated as

$$\kappa_2 = \frac{R_2^2 + R_1^2}{R_2^2 - R_1^2} \kappa_b. \tag{6}$$

After determining κ_2, the relationship between κ_0 and κ_1 according to equation (19) in literature [56] can be determined as

$$
\kappa_0 = \frac{\kappa_1 \cdot \left(\frac{(\kappa_2-\kappa_b)\cdot((\kappa_1+\kappa_2)\cdot R_1^2+(\kappa_2-\kappa_1)\cdot R_0^2)\cdot R_2^2}{(\kappa_2+\kappa_b)\cdot R_1^2} - ((\kappa_2 - \kappa_1) \cdot R_1^2 + (\kappa_1 + \kappa_2) \cdot R_0^2) \right)}{(\kappa_2 - \kappa_1) \cdot R_1^2 - (\kappa_1 + \kappa_2) \cdot R_0^2 - \frac{(\kappa_2-\kappa_b)\cdot((\kappa_1+\kappa_2)\cdot R_1^2-(\kappa_2-\kappa_1)\cdot R_0^2)\cdot R_2^2}{(\kappa_2+\kappa_b)\cdot R_1^2}}.
$$

$$ \tag{7}$$

Thermal cloaks don't require thermal conductivity of region 1, so we can determine κ_0 according to Eq. (7) when κ_2 meet param-

eter requirements of bilayer thermal cloaks and κ_1 is a non-zero constant value.

The numerical simulation results of the bilayer thermal encoding in a steady-state are presented in Fig. 4(b). The specific parameters used in Fig. 4(b) are $R_0 = 1$ cm, $R_1 = 1.5$ cm, $R_2 = 2$ cm, and the dimensions of the whole plane are 10×60 cm². The background thermal conductivity is $\kappa_b = 100$ Wm⁻¹ K⁻¹, and the thermal conductivities of the rest positions are set according to Eqs. (5)–(7). The encoded array consists of two forms of units staggered, with the upper and lower boundaries of the units being insulated. In Fig. 4(b) I–III, we gradually increase the temperature of the left and right boundaries of the encoding array, and the output value changes from (1,0,1,0,1,0) to (0,1,0,1,0,1). The encoding results of Fig. 4(b) I and III are completely opposite because the temperature of the unit in Fig. 4(b) I is all below the critical temperature, while the temperature of the unit in Fig. 4(b) III is all above the critical temperature. Half of the encoding units in Fig. 4(b) II are in the high-temperature state and half in the low-temperature state, and the encoding output is (1,0,1,1,0,1). The temperature gradients in the center and background regions of the unit in Fig. 4(b) are illustrated in Fig. 4(c), showing an apparent alternate arrangement result. Since the temperature difference between the left and right boundaries of the encoding array is maintained at 100 K, the background temperature gradient of each encoding array is consistent. We use a set of background temperature gradient values as reference values. When the encoding structure is fixed, the output value of the encoding can change with temperature, realizing a programmable encoding. The bilayer structure encoded array is valid for individual manipulation, and the simulation results are shown in Appendix A4. The finite element simulation confirms that the encoding design based on a temperature-dependent scattering cancellation scheme is effective.
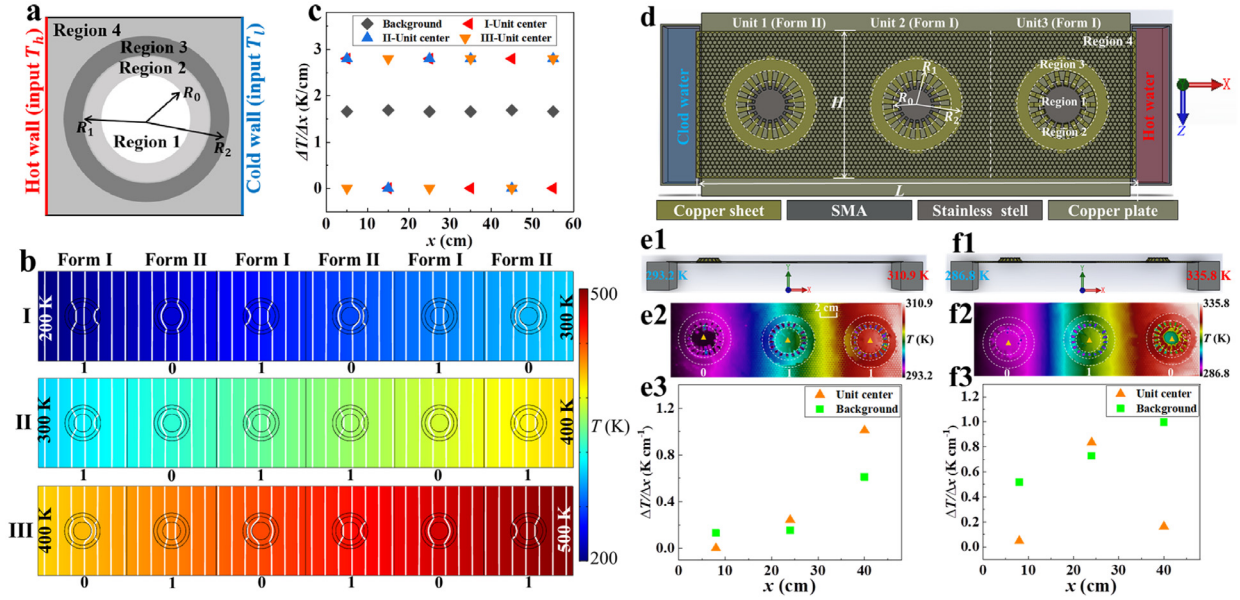
Fig. 4. Design and experimental results of thermal encoding based on temperature-dependent scattering cancellation theory. (a) Schematic diagram of bilayer temperature-controlled encoding unit structure. (b) The steady-state simulation results of bilayer temperature-controlled encoding array under batch control. (c) The temperature gradient in units' central and background regions in (b). (d) Top view of a temperature-controlled thermal encoding device. (e1) and (f1) are front views of the device at different temperatures. (e2) and (f2) are experimental results corresponding to (e1) and (f1), color surfaces represent temperature distribution. (e3) and (f3) show the temperature gradient values of the central region and background region of each unit in (e2) and (f2), respectively.

4.2. Experimental results

When there is a change in ambient temperature, the metamaterial's function automatically transforms from a cloak (or concentrator) to a concentrator (or cloak). To form a temperature-controlled thermal encoding device, we arrange the designed smart materials into rows. Fig. 4(d) (actual picture in Fig. A5(a) in Appendix) illustrates the top view of the experimental device, which is based on a copper sheet. The parameters in Fig. 4(d) are as follows: $L = 48$ cm, $H = 16$ cm, $R_0 = 2.6$ cm, $R_1 = 3.7$ cm, and $R_2 = 4.9$ cm. The left and right ends of the copper sheet are bent and then extend into cold water and hot water, respectively. The third region of each unit is made of copper, and the thermal conductivity is $\kappa_2 = 394$ Wm^{-1} K^{-1}. Considering Eq. (6) and the overall dimensions R_1 and R_2, we determine that the background thermal conductivity should be $\kappa_b = 117$ Wm^{-1} K^{-1}. To achieve this, we punch more than four thousand holes in region 4 and apply the formula $\kappa_b = P\kappa_{Cu} + (1 - P)\kappa_{air}$, where P is the volume fraction of metals and κ_{air} is the thermal conductivity of air. We place a layer of plastic film on the copper sheet to prevent heat loss caused by the convection of air in the hole with the environment. To enable the thermal conductivity of region 2 to switch between 0 and κ_1 at different temperatures, where κ_1 satisfies Eq. (7), we alternate two types of sheets along the tangential direction to raise the temperature gradient in the central zone and achieve the effect of the concentrator. In this ring, we design 18 copper teeth to be evenly arranged around the center of the circle, and the part without copper teeth is filled with air. The proportion of copper and air is the same. According to the effective medium theory [57,58], the effective conductivity κ_1 of such a laminated structure in region 2 is 3.24 Wm^{-1} K^{-1}, approximated by $\kappa_1 = \sqrt{\kappa_{Cu}\kappa_{air}}$. We then attach shape memory alloys (SMAs) to the copper teeth so that the deformation of the SMA drove the deformation of the copper teeth at different temperatures. Two SMAs are used in this experiment, corresponding to Form I and Form II in Eq. (5), respectively. In Fig. 4(d), unit 1 uses SMAs corresponding to Form II, and unit 2 and unit 3 use SMAs corresponding to Form I. When the tempera-

ture passing through SMA is higher than the phase transition temperature, SMA corresponding to Form II (Form I) straightens (bends upward). When the temperature is lower than the phase transition temperature, SMA bends upwards (straightens). If SMA bends upwards, it will drive the copper teeth of region 2 to bend upwards, so $\kappa_1 = \kappa_{air}$ approaches 0, which meets the requirements of cloaks. When SMA is straightened, the copper sheet is put down, and the laminated structure meets the requirements of concentrators. The phase transition temperature of the two SMA forms used here is 298.2 K, which has opposite phase transition directions. In practice, the SMA deformation at temperatures close to 298.2 K is too small to change the shape of the copper teeth in region 2 for functional switching. The SMA's temperature often needs close to 308.2 K for effect to be more prominent. Here κ_0 only needs to meet the requirements of concentrators since cloaks have no requirement for κ_0. According to Eq. (7), $\kappa_0 = 14.78$ Wm^{-1} K^{-1}, a stainless steel film is used in our experiment. Finally, the entire copper sheet is fixed on the copper plate to help transfer the heat of the copper sheet.

To demonstrate the repeatable encoding characteristics of temperature-controlled thermal encoding, we vary the temperature of the cold and heat source to produce different compilation results. The front view of the experimental device at different temperatures is depicted in Fig. 4(e1) and (f1) to provide a more intuitive visualization of the SMA lifting situation (refer to Fig. A5(b) and (c) of Appendix for the actual picture). Corresponding temperature distribution graphs for Fig. 4(e1) and (f1) are shown in Fig. 4(e2) and (f2), respectively. At a left boundary temperature of 293.2 K and a right boundary temperature of 310.9 K, the SMA of unit 1 is tilted upwards, corresponding to a cloak, while the SMA of units 2 and 3 are straight and flat, corresponding to a concentrator. The isotherm of the entire background in Fig. 4(e2) is straight, and the temperature in region 1 of unit 1 is significantly lower than the surrounding temperature. The isotherms in region 1 of units 2 and 3 tend to converge toward the center of the unit. For signal output, we read the temperature gradient value at the center point. Since the background heat flux density of the entire device

is non-uniform due to the influence of environmental convection, we select the temperature gradient of each unit for signal output. We calculate the temperature gradient $\Delta T/\Delta x$ of the center area and the background area for each unit and plot it in Fig. 4(e3) and (f3) corresponding to Fig. 4(e2) and (f2), respectively. For calculation details, refer to Appendix A6. A higher (lower) temperature gradient at the unit's center than its reference value indicates an output code value of 1 (0), respectively. Thus, the output encode value in Fig. 4(e3) is (0,1,1). When the left and right boundary temperatures are 286.8 K and 335.8 K in Fig. 4(f2), respectively, the SMA of units 1 and 3 are tilted, and the SMA of unit 2 is straightened. Figure 4(f3) shows that the temperature gradient at the center point of unit 1 and unit 3 is lower than their reference value, while unit 2 is higher than its reference value, resulting in an output encode value of (0,1,0). Although the cloak's effect cannot be seen intuitively in unit 1 of Fig. 4(f2) because the temperature of the cold source is lower than the ambient temperature (293.2 K), and the temperature of the copper plate as the bottom plate is transmitted to the stainless steel in region 1, the absence of an isotherm entering region 1 confirms that it is still a cloak. Figure 4(f3) also supports this result. Thus, we have demonstrated the adjustability and repeatability of temperature-controlled thermal encoding. We can reuse a designed thermal encoding device and change the output encoding value by adjusting the temperature. We can even individually control the temperature of each unit to achieve more output results.

5. Conclusion

We present a novel programmable encoding strategy for macroscopic diffusion systems, which is the first of its kind. Our approach utilizes a refined temperature-responsive configuration design and an elaborate control of local temperature to localize, distinguish, program, and read thermal signals, demonstrating the possibility of digital encoding in purely diffusive processes. Our design achieves programmability without the need for complex installations or additional fields for unit control, making it a more efficient and robust encoding scheme than existing thermal encoding methods [36–38]. We verify the robustness of our design through numerical simulations under both steady and transient environments, and a proof-of-principle prototype is experimentally fabricated to illustrate the encoding process. Our strategy employs classical metamaterial design methods, including transformation thermotics and scattering-cancellation technology, which improve the completeness and feasibility of the programmable encoding. Our thermal coding strategy can even be extended to ternary or multivariate encodings if we consider merging a wider range of functions. A continuously tunable structure [22–24] enables ternary encoding (cloak, concentrator, and transparency) and multielement encoding by carefully setting multiple temperature gradient reference steps. The propose underlying fundamental and implementation model promisingly promote a new territory–thermal information metamaterial, and paves a gorgeous way for information processing and encoding in diffusion systems.

Declaration of Competing Interest

Authors declare that they have no conflict of interest.

CRediT authorship contribution statement

Min Lei: Formal analysis, Writing – original draft. **Chaoran Jiang:** Formal analysis. **Fubao Yang:** Formal analysis, Writing – original draft. **Jun Wang:** Conceptualization, Formal analysis, Writing – original draft. **Jiping Huang:** Conceptualization, Formal analysis, Writing – original draft.

Data availability

Data will be made available on request.

Acknowledgments

Appendix A

A1. Proof of form–invariance of heat conduction equation and derivation of transformation rules

Temperature-dependent transformation thermotics means that transformed thermal conductivity is temperature-dependent, including two cases where background thermal conductivity is temperature-dependent or coordinate transformation is temperature-dependent. Here we consider that background thermal conductivity is temperature-independent, but the coordinate transformation is temperature-dependent. According to Fourier's law, governing equation of heat conduction without a heat source can be described as

$$\rho C \frac{\partial T}{\partial t} = \nabla \cdot (\boldsymbol{\kappa} \cdot \nabla T), \tag{A1}$$

where $\boldsymbol{\kappa}$ is the temperature-independent thermal conductivity tensor. Now we are in the position to prove that governing equation Eq. (A1) satisfies form invariance under arbitrary temperature-dependent coordinate transformation so that the temperature-dependent transformation theory is still valid. In a temperature-dependent curvilinear coordinate system with a set of contravariant basis $\{\boldsymbol{g}^i(T), \boldsymbol{g}^j(T), \boldsymbol{g}^k(T)\}$, a group of covariant basis $\{\boldsymbol{g}_i(T), \boldsymbol{g}_j(T), \boldsymbol{g}_k(T)\}$, and corresponding contravariant components $(x^i(T), y^j(T), z^k(T))$, the governing equation of heat conduction can be reproduced as

$$\sqrt{g(T)}\rho C \frac{\partial T}{\partial t} - \partial_i(\sqrt{g(T)}\sigma^{ij}(T)\partial_j T) = 0, \tag{A2}$$

where $g(T)$ is the determinant of the matrix with components $g_{ij}(T) = \boldsymbol{g}_i(T) \cdot \boldsymbol{g}_j(T)$. Eq. (A2) shows that the Fourier law of heat conduction expressed by the tensor component has no formal difference in different coordinate systems, even temperature-dependent coordinate systems, except that the coefficient $\sqrt{g(T)}$ is different. According to Eq. (A2), we verify the form invariance of Eq. (A1).

To obtain the transformation rules of material properties, We consider a bijection from pretransformed space (virtual space) with a chosen set of curvilinear coordinates $\{x, y, z\}$ to a transformed space (physical space) with another set of Cartesian coordinates $\{x'(T), y'(T), z'(T)\}$, the governing equation can be rewritten as

$$\rho'(T)C' \frac{\partial T'}{\partial t} = \nabla' \cdot \left(\boldsymbol{\kappa}'\left(T'\right) \cdot \nabla' T'\right), \tag{A3}$$

where $\boldsymbol{\kappa}'(T)$ is the temperature-dependent thermal conductivity tensor after a temperature-dependent coordinate transformation.

By comparing Eqs. (A2) and (A3), the transformed thermal conductivity, density, and thermal capacity can be expressed as

$$\boldsymbol{\kappa}'(T') = \frac{A(T)\kappa_0 A^{\mathrm{tr}}(T)}{\det A(T)},$$

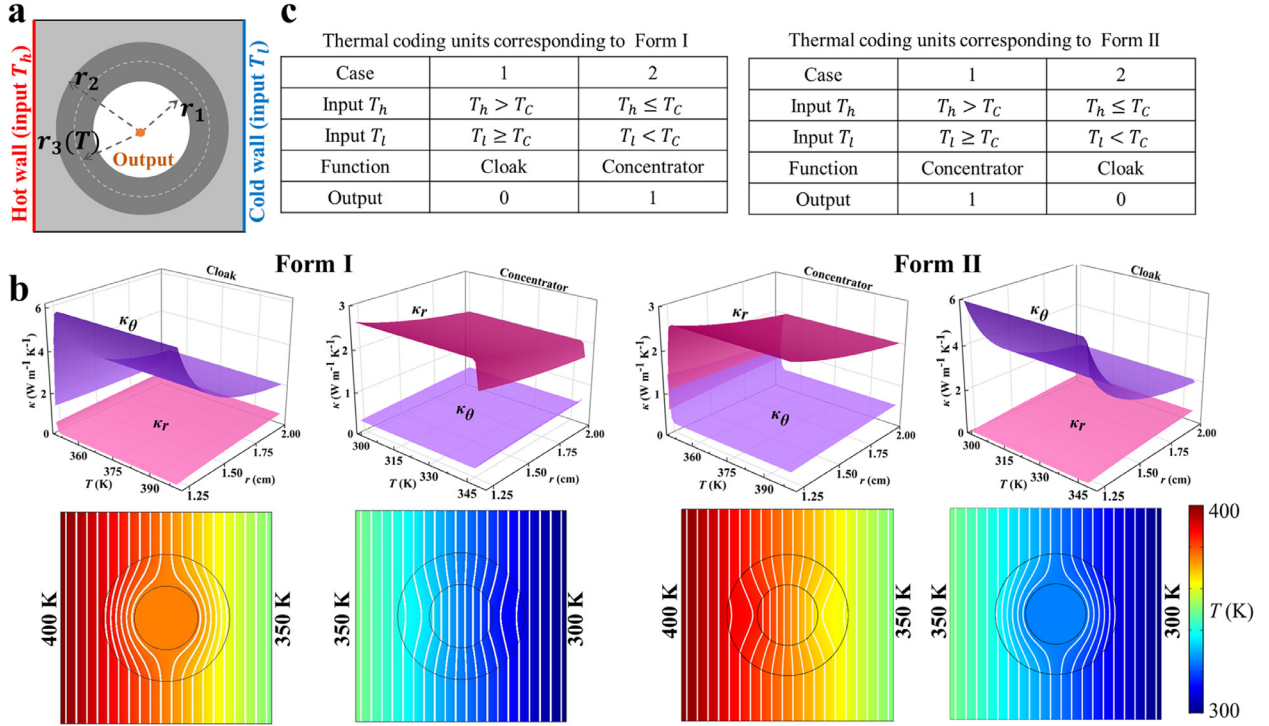$$\rho'(T) = \frac{\rho}{\det A(T)},$$

Fig. A1. Definition and simulation results of two forms of temperature-controlled thermal encoding units. (a) The structure of the encoding unit. (b) Thermal conductivity distribution and temperature distribution at the high and low temperature of the two form units, where the phase transition temperature of both units is 350 K. (c) The relationship between the input and output of the two form units.
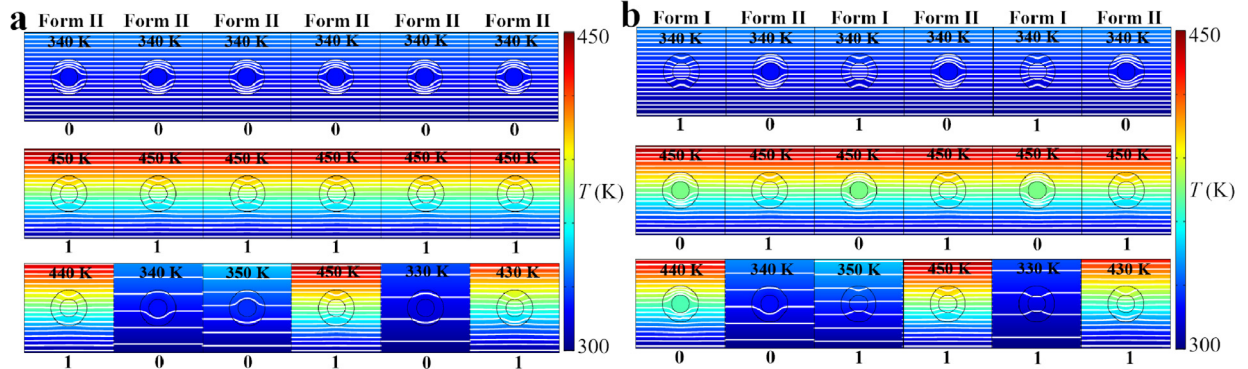

Fig. A2. Separate manipulation results of the encoding array in a steady state. (a) The encoding array consists of 6 units of Form II. (b) The encoding array consists of two form units interleaved. All units have a bottom boundary temperature of 300 K and a phase transition temperature of 350 K.

$$C' = C, \tag{A4}$$

where $\kappa'(T)$ is temperature-dependent thermal conductivity of device, κ_0 is temperature-independent thermal conductivity of background, $A(T)$ is temperature-dependent Jacobian matrix, $A^{tr}(T)$ is transpose of $A(T)$, and $\det A(T)$ is determinant of $A(T)$.

Next, we consider a temperature-dependent coordinate transformation that enables functional switching. We consider the coordinate transformation of a traditional thermal concentrator. A thermal concentrator can enhance heat flow in a specific area without changing background heat flow distribution. Its coordinate transformation can be expressed as:

$$
\begin{aligned}
r' &= r_1 r/r_3 \quad (r' < r_1), \\
r' &= r(r_2 - r_1)/(r_2 - r_3) \\
&\quad + r_2(r_1 - r_3)/(r_2 - r_3) \quad (r_1 < r' < r_2), \\
\theta' &= \theta,
\end{aligned}
\tag{A5}
$$

where r_1 and r_2 are the inner radii and outer radius of a thermal concentrator, r_3 is the radius between r_1 and r_2, as shown in Fig. A1(a). The physical meaning of coordinate transformation is to compress a circular area with radius r_3 into a circular area with radius r_1, and the annular areas with inner radius r_3 and outer radius r_2 are stretched into annular areas with inner radius r_1 and outer radius r_2, respectively. If $r_3 = 0$, the coordinate transformation of thermal concentrators can be transformed into the coordinate transformation of thermal cloaks

$$r' = r\frac{r_2 - r_1}{r_2} + r_1, \quad \theta' = \theta. \tag{A6}$$

The coordinate transformation of the cloak is to compress a circular region with a radius r_2 into the annulus region with a radius between r_1 and r_2. A thermal cloak can prevent heat flow from entering a specific area without disturbing background thermal field distribution, so it is impossible to know the information of the specific area by conducting heat detection outside.
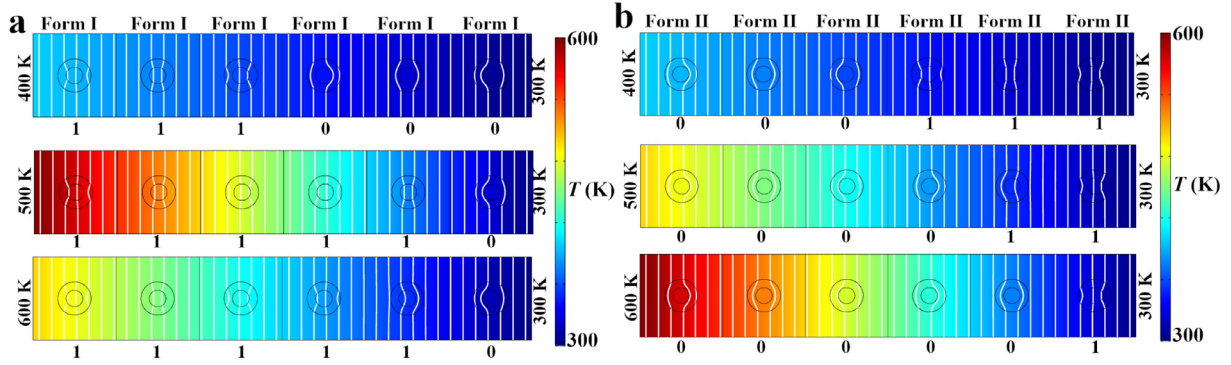
Fig. A3. Batch manipulation results of encoded arrays in steady state. (a) The encoding array consists of 6 units of Form I. (b) The encoding array consists of 6 units of Form II. The phase transition temperature of all units is 350 K.
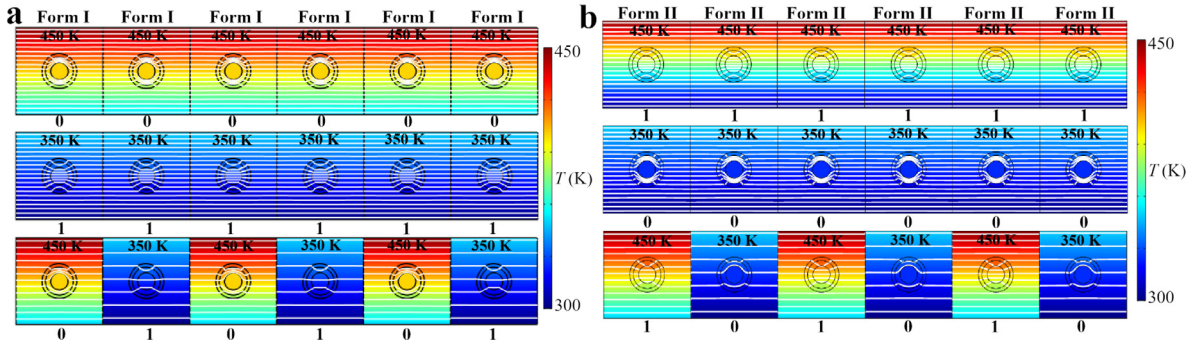

Fig. A4. Results of separate manipulation of encoded arrays with bilayer structures in steady state. (a) The encoding array consists of 6 units of Form I. (b) The encoding array consists of 6 units of Form II. All units have a bottom boundary temperature of 300 K and a phase transition temperature of 350 K.

If r_3 is temperature-dependent, we can switch between cloak and concentrator functions. The temperature-dependent coordinate $r_3(T)$ can be written as

$$r_3(T) = \frac{r_3}{1 + \exp \eta (T - T_C)} \quad \text{(Form I)},$$

$$r_3(T) = \frac{r_3 \exp \eta (T - T_C)}{1 + \exp \eta (T - T_C)} \quad \text{(Form II)}, \tag{A7}$$

where $r_3(T)$ has two temperature-dependent forms. Temperature-dependent coordinate $r_3(T)$ determines the direction of phase-change behavior so that these two forms of thermal encoding have inverse encode numbers under the same environments. Replace r_3 in Eq. (A5) with $r_3(T)$, Eq. (A5) can be rewritten as

$$r' = r_1 r / r_3(T) \quad (r' < r_1),$$
$$r' = r(r_2 - r_1)/(r_2 - r_3(T))$$
$$\quad + r_2(r_1 - r_3(T))/(r_2 - r_3(T)) \quad (r_1 < r' < r_2),$$
$$\theta' = \theta. \tag{A8}$$

If we consider Form 1 (Form II) in Eq. (A7), it is easy to see that when the ambient temperature is higher than and lower than the critical temperature, Eq. (A8) corresponds to coordinate transformation of cloaks (concentrators) and concentrators (cloaks), respectively. Substituting Eq. (A8) into Eq. (A4), transformed thermal conductivity and density of shell region with inner radius r_1 and outer radius r_2 in Fig. A1(a) can be written as

$$\kappa'(T) = \kappa_0 \begin{bmatrix} 1 + \frac{(r_3^*(T) - r_1) r_2}{(r_2 - r_3^*(T)) r'} & 0 \\ 0 & (1 + \frac{(r_3^*(T) - r_1) r_2}{(r_2 - r_3^*(T)) r'})^{-1} \end{bmatrix},$$

$$\rho' = \frac{(r_2 - r_3(T))^2 r' - (r_2 - r_3(T))(r_1 - r_3(T)) r_2}{(r_2 - r_1)^2 r'}. \tag{A9}$$

Transformed thermal conductivity and density of circular region with radius r_1 in Fig. A1(a) can be expressed as

$$\kappa'(T) = \kappa_0 \begin{bmatrix} 1 & 0 \\ 0 & 1 \end{bmatrix},$$

$$\rho' = \rho (r_3(T)/r_1)^2. \tag{A10}$$

The transformed thermal conductivity distribution corresponds to two forms of $r_3(T)$, shown in Fig. A1(b). We plug the calculated thermal conductivity into COMSOL Multiphysics software to draw the temperature distribution map. The inner radius of the transformed layer in Fig. A1(b) is $r_1 = 1$ cm, the outer radius is $r_2 = 2$ cm, and the virtual radius is $r_3 = 1.5$ cm. The phase transition temperature of both types of units is 350 K. For Form I (Form II), tangential thermal conductivity is higher (lower) than radial thermal conductivity when the unit temperature is higher than the phase transition temperature, and the output is a cloak (concentrator). If the unit temperature is lower than the phase transition temperature, the tangential thermal conductivity is lower (higher) than the radial thermal conductivity; the output is a concentrator (cloak). We define the output encode number 0 (1) when the result is a cloak (concentrator). According to the definition of encoded values, we summarize the relationship between the input and output of the two formal units, which is shown in Fig. A1(c).

Based on these definitions, we summarize the relationship between the input and output of the two formal units in Fig. A1(c).

A2. Simulation results of individual manipulation on encoding arrays in steady state

The encoding array, which is controlled separately in the main text, consists of units of Form I, allowing for the programmability of the encoding array. We demonstrate that an encoding array composed of units of Form II and an encoding array that
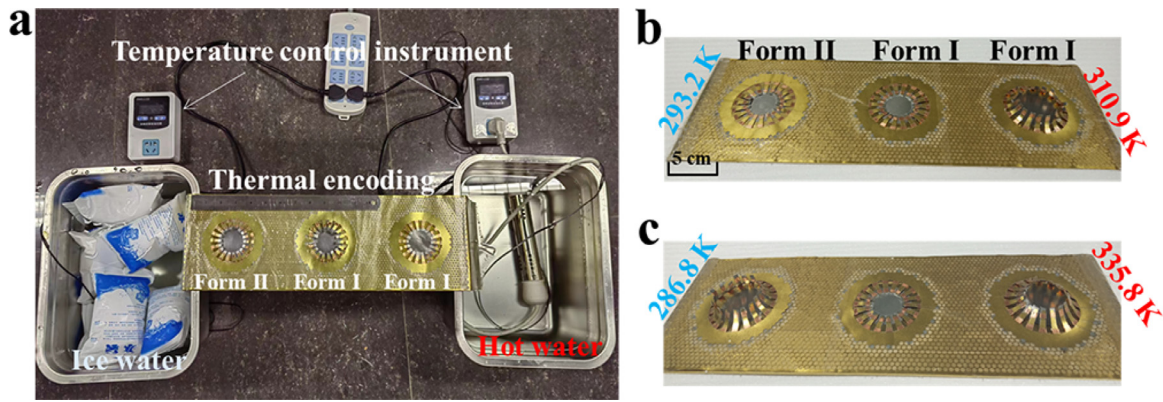
Fig. A5. (a) Physical drawings of the experimental facility. (b) and (c) Experimental results at different temperatures.
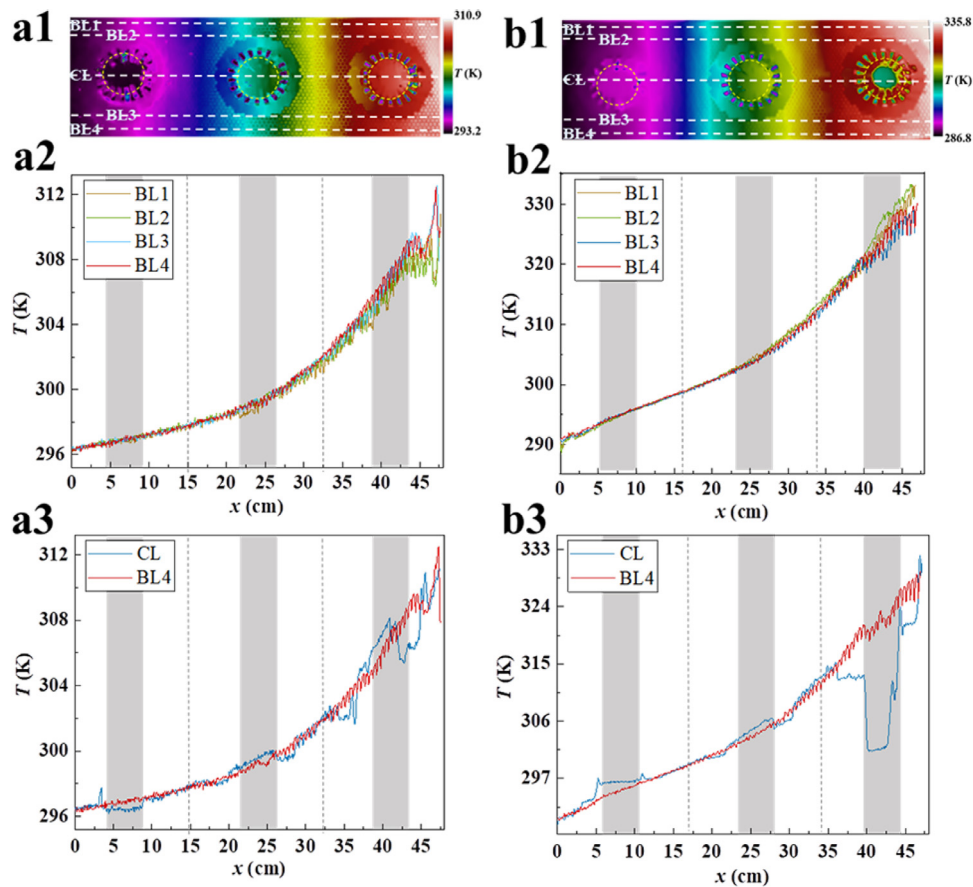

Fig. A6. (a1)-(b1) Temperature distribution diagram of the encoding equipment under different conditions. (a2)-(b2) Temperature distribution in the background region of (a1)-(b1). (a3)-(b3) Comparison of temperature maps between the background region and the central region.

interleaves two forms of units can also achieve programmability through separate manipulation. The results are presented in Fig. A2, and the geometric dimensions and boundary conditions are the same as in Fig. 2(b) of the main text. The encoding array confirms the properties of phase transitions in opposite directions for units of Form II and Form I. Furthermore, the interleaved encoding array satisfies programmability, and the output results can be adjusted by temperature. It should be noted that the operating temperature range is limited in practice. Depending on the specific requirements, a combination of units of Form I and Form II can be

selected to form the encoding array to achieve a greater number of encoding results.

A3. Simulation results of batch manipulation on encoded arrays in steady state

Figure A3 shows that the encoding array consists of one form of units that can also achieve multiple encoding outputs in batch manipulation. When the encoding array is made up of units from Form I, the encoding value 0 decreases while 1 increases as the left

boundary temperature rises. This occurs because the unit of Form I functions as a concentrator in the high-temperature state, resulting in an output of 1. Conversely, the encoding array formed by units of Form II yields results opposite to those of Form I.

A4. Simulation results of individual manipulation on the encoding arrays consisting of bilayer coding units

Figure A4 proves that the bilayer structure thermal encoding based on the temperature-dependent scattering cancellation theory can also achieve programmability in a separate operation. The left and right boundaries of each unit in Fig. A4 are set as thermal insulation, and the output encoded value is changed by adjusting the unit's upper boundary temperature. The output of Fig. A4(a) and (b) are opposite under the same boundary conditions.

A5. Real pictures of experimental setups

Figure A5 (a) depicts the complete physical setup of the thermal encoding equipment. The left and right ends of the equipment are curved and connected to cold and hot water sources, respectively. An ice-water mixture is utilized as the cold source, and a temperature control device is employed to monitor the temperature of the cold source in real-time. The ice-water mixture can sustain a constant temperature for an extended duration, with temperature fluctuations remaining within 0.5 K per hour. The heat source is generated by inserting a heating rod into cold water, which heats the water to the desired temperature. The temperature control device is programmed to activate the heating rod when the heat source temperature falls below the set temperature, and it automatically switches it off once the desired temperature is achieved. This ensures that the heat source remains at a constant temperature throughout the experiment. The entire experiment is conducted in an air-conditioned room, located far from the outlet, to maintain a constant ambient temperature and minimize the impact of ambient convection.

Figure A5 (b) and (c) illustrate the oblique view of the fabricated thermal encoding array. Unit 1 has different states at different temperature regions to achieve specific output results, while the other two units keep invariant. This phenomenon occurs due to the variation of local temperatures at unit 2 and 3, which are located on one side of their respective phase-change points, resulting in robust encoding numbers. The binary encoding numbers are particularly robust as each unit cell only has a single phase-change point.

A6. Extraction method of temperature gradient values in experiment

Figure 4 (e2) and (f2) in the main text display the temperature distribution maps. Although the background isotherm appears to be basically straight and there is a difference between the cloak and the concentrator in the central area, this judgment is not precise enough. To validate the result of each unit, we select four background lines (BL1–BL4) in Fig. A6(a1) and (b1) to create their corresponding line maps. In Fig. A6(a2) and (b2), we observe that the temperature distributions of the four background lines are essentially identical. Therefore, we can select any of the background lines as our reference line. To compare with the reference line (BL4), we create a line graph of the center line (CL) shown in Fig. A6(a3) and (b3). The gray area in the figure corresponds to the central area of each unit in the temperature distribution graph. We see that CL and the BL4 in the background area are nearly identical, indicating that the background temperature distribution is undisturbed. By calculating the slope of the temperature graph, we can determine whether the result is a cloak or a concentrator. Next, we select the data in the gray area to conduct linear fitting to obtain

slopes, which represent the temperature gradient. The results are shown in Fig. 4(e3) and (f3) of the main text. In the experiment, we do not use temperature as the criterion for judgment. This is because the stainless steel in the center area is placed in the air. When the SMA is lifted, the temperature of the copper sheet is not transmitted to the stainless steel, and the temperature of the stainless steel will be close to the ambient temperature. Therefore, the temperature in the central area of the cloak may not be lower than the background temperature.

References

[1] S.C. Brown, F.I. Craik, Encoding and Retrieval of Information, Oxford University Press, 2000.
[2] R.V. Hartley, Transmission of information, Bell Syst. Tech. J. 7 (1928) 535–563.
[3] T. Schreiber, Measuring information transfer, Phys. Rev. Lett. 85 (2000) 461.
[4] H. Borko, Information science: what is it? Am. Doc. 19 (1968) 3–5.
[5] B.C. Brookes, The foundations of information science. part I. Philosophical aspects, J. Inf. Sci. 2 (1980) 125–133.
[6] A. Bejan, Evolution in thermodynamics, Appl. Phys. Rev. 4 (2017) 011305.
[7] N. Li, J. Ren, L. Wang, G. Zhang, P. Hänggi, B.W. Li, Colloquium: phononics: manipulating heat flow with electronic analogs and beyond, Rev. Mod. Phys. 84 (2012) 1045.
[8] M. Maldovan, Sound and heat revolutions in phononics, Nature 503 (2013) 209.
[9] B. Li, L. Wang, G. Casati, Thermal diode: rectification of heat flux, Phys. Rev. Lett. 93 (2004) 184301.
[10] W.X. Zhao, Z. Zhu, Y.W. Fan, W. Xi, R. Hu, X.B. Luo, Temporally-adjustable radiative thermal diode based on metal-insulator phase change, Int. J. Heat Mass Transf. 185 (2022) 122443.
[11] L. Wang, B.W. Li, Thermal logic gates: computation with phonons, Phys. Rev. Lett. 99 (2007) 177208.
[12] L. Wang, B.W. Li, Thermal memory: a storage of phononic information, Phys. Rev. Lett. 101 (2008) 267203.
[13] T.J. Cui, M.Q. Qi, X. Wan, J. Zhao, Q. Cheng, Coding metamaterials, digital metamaterials and programmable metamaterials, Light Sci. Appl. 3 (2014) e218.
[14] L. Zhang, X.Q. Chen, S. Liu, Q. Zhang, J. Zhao, J.Y. Dai, G.D. Bai, X. Wan, Q. Cheng, G. Castaldi, V. Galdi, T.J. Cui, Space-time-coding digital metasurfaces, Nat. Commun. 9 (2018) 4334.
[15] C.Z. Fan, Y. Gao, J.P. Huang, Shaped graded materials with an apparent negative thermal conductivity, Appl. Phys. Lett. 92 (2008) 251907.
[16] S. Narayana, Y. Sato, Heat flux manipulation with engineered thermal materials, Phys. Rev. Lett. 108 (2012) 214303.
[17] R. Hu, S.L. Zhou, Y. Li, D.Y. Lei, X.B. Luo, C.W. Qiu, Illusion thermotics, Adv. Mater. 30 (2018) 1707237.
[18] T.C. Han, P. Yang, Y. Li, D.Y. Lei, B.W. Li, K. Hippalgaonkar, C.W. Qiu, Full-prameter omnidirectional thermal metadevices of anisotropic geometry, Adv. Mater. 30 (2018) 1804019.
[19] R. Hu, S.Y. Huang, M. Wang, X.B. Luo, J. Shiomi, C.W. Qiu, Encrypted thermal printing with regionalization transformation, Adv. Mater. 31 (2019) 1807849.
[20] Z. Zhu, X.C. Ren, W. Sha, M. Xiao, R. Hu, X.B. Luo, Inverse design of rotating metadevice for adaptive thermal cloaking, Int. J. Heat Mass Transf. 176 (2021) 121417.
[21] T.C. Han, X.L. Yue, K.H. Wen, J.Y. Nangong, Monolayer thermal meta-device with switching functions, Int. J. Heat Mass Transf. 186 (2022) 122498.
[22] G.Q. Xu, K.C. Dong, Y. Li, H.G. Li, K.P. Liu, L.Q. Li, J.Q. Wu, C.W. Qiu, Tunable analog thermal material, Nat. Commun 11 (2020) 6028.
[23] J.X. Li, Y. Li, P.-C. Cao, T.Z. Yang, X.-F. Zhu, W.Y. Wang, C.W. Qiu, A continuously tunable solid-like convective thermal metadevice on the reciprocal line, Adv. Mater. 32 (2020) 2003823.
[24] P. Jin, J.R. Liu, L.J. Xu, J. Wang, X.P. Ouyang, J.H. Jiang, J.P. Huang, Tunable liquid-solid hybrid thermal metamaterials with a topology transition, Proc. Natl. Acad. Sci. USA 120 (2023). E2217068120
[25] S. Yang, J. Wang, G.L. Dai, F.B. Yang, J.P. Huang, Controlling macroscopic heat transfer with thermal metamaterials: theory, experiment and application, Phys. Rep. 908 (2021) 1.
[26] Y. Li, W. Li, T.C. Han, X. Zheng, J.X. Li, B.W. Li, S.H. Fan, C.W. Qiu, Transforming heat transfer with thermal metamaterials and devices, Nat. Rev. Mater. 6 (2021) 488.
[27] Z. Zhang, L. Xu, T. Qu, M. Lei, Z.-K. Lin, X. Ouyang, J.-H. Jiang, J. Huang, Nat. Rev. Phys. In press (2023).
[28] Z.C. Wang, Z. Zhu, T.F. Liu, R. Hu, Inverse design of thermal metamaterials with holey engineering strategy, J. Appl. Phys 132 (2022) 145102.
[29] W. Sha, M. Xiao, J.H. Zhang, X.C. Ren, Z. Zhu, Y. Zhang, G.Q. Xu, H.G. Li, X.L. Liu, X. Chen, L. Gao, C.-W. Qiu, R. Hu, Robustly printable freeform thermal metamaterials, Nat. Commun. 12 (2021) 7228.
[30] R. Hu, W. Xi, Y.D. Liu, K.C. Tang, J.L. Song, X.B. Luo, J.Q. Wu, C.W. Qiu, Thermal camouflaging metamaterials, Mater. Today 45 (2021) 120–141.
[31] Y. Li, X.Y. Shen, Z.H. Wu, J.Y. Huang, Y.X. Chen, Y.S. Ni, J.P. Huang, Temperature-dependent transformation thermotics: from switchable thermal cloaks to macroscopic thermal diodes, Phys. Rev. Lett. 115 (2015) 195503.

[32] X.Y. Shen, Y. Li, C.R. Jiang, J.P. Huang, Temperature trapping: energy-free maintenance of constant temperatures as ambient temperature gradients change, Phys. Rev. Lett. 117 (2016) 055501.

[33] X.Y. Shen, Y. Li, C.R. Jiang, Y.S. Ni, J.P. Huang, Thermal cloak-concentrator, Appl. Phys. Lett. 109 (2016) 031907.

[34] J. Wang, J. Shang, J.P. Huang, Negative energy consumption of thermostats at ambient temperature: electricity generation with zero energy maintenance, Phys. Rev. Appl. 11 (2019) 024053.

[35] Y.Y. Li, H.C. Zhang, Y.J. Chen, D. Zhang, Z.L.g. Huang, H.M. Wang, Realization and analysis of an intelligent flux transfer regulator by allocating thermal and DC electric fields, Int. J. Heat Mass Transf. 179 (2021) 121677.

[36] R. Hu, S.Y. Huang, M. Wang, L.L. Zhou, X.Y. Peng, X.B. Luo, Binary thermal encoding by energy shielding and harvesting units, Phys. Rev. Appl. 10 (2018) 054032.

[37] X. Zhou, G.Q. Xu, Self-adaptive field manipulation with thermal logic material, Int. J. Heat Mass Transf. 172 (2021) 121147.

[38] Z.F. Xu, L.Q. Li, X.C. Chang, Y. Zhao, W.Y. Wang, Thermal field manipulation via a two-phase thermal metamaterial, Appl. Mater. Today 22 (2021) 100911.

[39] J.Y. Li, Y. Gao, J.P. Huang, A bifunctional cloak using transformation media, J. Appl. Phys. 108 (2010) 074504.

[40] Y.G. Ma, Y.C. Liu, M. Raza, Y.D. Wang, S.L. He, Experimental demonstration of a multiphysics cloak: manipulating heat flux and electric current simultaneously, Phys. Rev. Lett. 113 (2014) 20550.

[41] C.W. Lan, B. Li, J. Zhou, Simultaneously concentrated electric and thermal fields using fan-shaped structure, Opt. Express 23 (2015) 24475–24483.

[42] T.Z. Yang, X. Bai, D.L. Gao, L.Z. Wu, B.W. Li, J.T.L. Thong, C.W. Qiu, Invisible sensors: simultaneous sensing and camouflaging in multiphysical fields, Adv. Mater. 27 (2015) 7752–7758.

[43] X.W. Zhang, X. He, L.Z. Wu, A bilayer thermal-electric camouflage device suitable for a wide range of natural materials, Compos. Struct. 261 (2021) 113319.

[44] http://www.comsol.com/.

[45] T.C. Han, X. Bai, D.L. Gao, J.T.L. Thong, B.W. Li, C.W. Qiu, Experimental demonstration of a bilayer thermal cloak, Phys. Rev. Lett. 112 (2014) 054302.

[46] H.Y. Xu, X.H. Shi, F. Gao, H.D. Sun, B.L. Zhang, Ultrathin three-dimensional thermal cloak, Phys. Rev. Lett. 112 (2014) 054301.

[47] G.Q. Xu, X. Zhou, J.Y. Zhang, Bilayer thermal harvesters for concentrating temperature distribution, Int. J. Heat Mass Transf. 142 (2019) 118434.

[48] J.F. Ihlefeld, B.M. Foley, D.A. Scrymgeour, J.R. Michael, B.B. McKenzie, D.L. Medlin, M. Wallace, S. Trolier-McKinstry, P.E. Hopkins, Room-temperature voltage tunable phonon thermal conductivity via reconfigurable interfaces in ferroelectric thin films, Nano Lett. 15 (2015) 1791.

[49] F.Y. Yang, K. Liu, K. Hong, D.H. Reich, P.C. Searson, C.L. Chien, Large magnetoresistance of electrodeposited single-crystal bismuth thin films, Science 284 (1999) 1335.

[50] M.N. Baibich, J.M. Broto, A. Fert, F.N. Van Dau, F. Petroff, P. Etienne, G. Creuzet, A. Friederich, J. Chazelas, Giant magnetoresistance of (001)Fe/(001)Cr magnetic superlattices, Phys. Rev. Lett. 61 (1988) 2472.

[51] J. Kimling, R.B. Wilson, K. Rott, J. Kimling, G. Reiss, D.G. Cahill, Spin-dependent thermal transport perpendicular to the planes of Co/Cu multilayers, Phys. Rev. B 91 (2015) 144405.

[52] J. Cho, M.D. Losego, H.G. Zhang, H. Kim, J. Zuo, I. Petrov, D.G. Cahill, P.V. Braun, Electrochemically tunable thermal conductivity of lithium cobalt oxide, Nat. Commun. 5 (2014) 4035.

[53] J. Shin, J. Sung, M. Kang, X. Xie, B. Lee, K.M. Lee, T.J. White, C. Leal, N.R. Sottos, P.V. Braun, D.G. Cahill, Light-triggered thermal conductivity switching in azobenzene polymers, Proc. Natl. Acad. Sci. USA 116 (2019) 5973.

[54] C. McGuire, K. Sawchuk, A. Kavner, Measurements of thermal conductivity across the B1-B2 phase transition in NaCl, J. Appl. Phys. 124 (2018) 115902.

[55] A.V. Talyzin, O. Andersson, B. Sundqvist, A. Kurnosov, L. Dubrovinsky, High–pressure phase transition in LiBH4, J. Solid State Chem. 180 (2007) 510.

[56] T. Qu, J. Wang, J.P. Huang, Manipulating thermoelectric fields with bilayer schemes beyond Laplacian metamaterials, Europhys. Lett. 135 (2021) 54004.

[57] J.P. Huang, K.W. Yu, Enhanced nonlinear optical responses of materials: composite effects, Phys. Rep 431 (2006) 87.

[58] Y. Gao, J.P. Huang, Y.M. Liu, L. Gao, K.W. Yu, X. Zhang, Optical negative refraction in ferrofluids with magneto-controllability, Phys. Rev. Lett. 104 (2010) 034501.